SCIENCE CHINA
Information Sciences

• RESEARCH PAPER •

May 2023, Vol. 66 152303:1–152303:10
https://doi.org/10.1007/s11432-021-3495-y

Power-time resource allocation for downlink SWIPT-assisted cooperative NOMA systems

Chengpeng LIU, Lin ZHANG*, Zhi CHEN & Shaoqian LI

National Key Lab of Science and Technology on Communications, University of Electronic Science and Technology of China, Chengdu 611731*, China*

Received 23 December 2021/Revised 15 March 2022/Accepted 11 May 2022/Published online 20 April 2023

Abstract We study a downlink cooperative non-orthogonal multiple access (NOMA) system in which a base station (BS) serves two paired users on the same frequency band simultaneously, and the near user acts as an energy-constrained relay for the far user since there is no direct link between the BS and the far user due to physical obstacles or heavy shadowing. To replenish energy of the near user for relaying, we enable the near user to harvest energy from BS signals by adopting the simultaneous wireless information and power transfer (SWIPT) technique. Different from the linear energy harvesting (EH) model used in most of the existing literature, we adopt a non-linear model for EH. By considering the non-linear features of the practical circuits, we aim to minimize the BS energy consumption while ensuring the minimum required transmission rate of both users. Since the formulated problem contains coupled power and time resource variables, it is challenging to solve it directly. Thus, we propose an optimal power-time resource allocation algorithm by decoupling the variables properly. Simulation results verify the theoretical analysis and show the performance of the considered system.

Keywords NOMA, SWIPT, relaying, non-linear, transmit energy

Citation Liu C P, Zhang L, Chen Z, et al. Power-time resource allocation for downlink SWIPT-assisted cooperative NOMA systems. Sci China Inf Sci, 2023, 66(5): 152303, https://doi.org/10.1007/s11432-021-3495-y

1 Introduction

With the thriving of various applications such as autonomous driving and smart city, Internet of Things (IoT) has been playing a more and more important role in the modern society and is expected to support massive wireless connections and various services [1,2]. However, it is challenging for current radio access technology to accommodate these demands. Therefore, new multiple access techniques have been widely studied in recent years [3, 4].

Non-orthogonal multiple access (NOMA) is a promising multiple access strategy for IoT scenarios [5, 6]. In particular, Ref. [5] considered a downlink NOMA wireless network with multiple IoT users and investigated the dynamic user scheduling and power allocation to minimize the long-term power consumption of the whole system. Ref. [6] studied a satellite-integrated IoT with multiple users supporting by NOMA technique, and optimized the resource allocation from the perspective of improving user fairness to ensure quality of service. To enhance network coverage and reception reliability, the relay-assisted cooperative communication was introduced into NOMA [7–9]. Specifically, Ref. [7] adopted a dedicated relay to help the data transmissions between the base station (BS) and far user and derived the outage probabilities of users. Ref. [8] considered an NOMA network consisting of multiple users and a dedicated relay acted by a unmanned aerial vehicle, and maximized the network energy efficiency by optimizing power allocation. Ref. [9] studied the impact of the relay selection on the outage probability in a cooperative NOMA network with multiple dedicated relays. Alternatively, Refs. [10–12] enabled the near NOMA user to serve as a relay for the far user, which decreases the system cost.

However, IoT devices typically are equipped with small capacity battery due to size or cost limitations. It is obvious that cooperative relaying may consume extra energy of the near user acting as a relay and thus

* Corresponding author (email: linzhang1913@gmail.com)

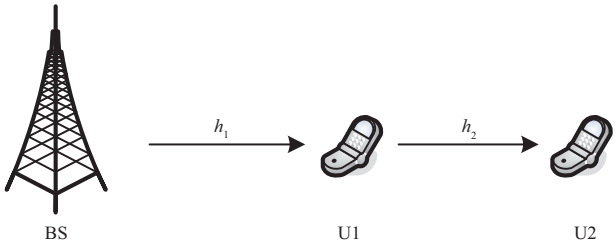

Figure 1 Downlink SWIPT-assisted cooperative NOMA system model.

severely shorten the network lifetime [13]. To alleviate the issue, the simultaneous wireless information and power transfer (SWIPT) technique was introduced into the cooperative NOMA systems [14–16]. When the SWIPT technique is adopted, there are two models for energy harvesting (EH). One is a linear model that the output power of the harvester is directly proportional to the input power, which is adopted in most of the existing literature [14,15]. In particular, Ref. [14] studied a user-aided cooperative SWIPT NOMA system and maximized the system energy efficiency. Ref. [15] investigated a SWIPT-enabled cooperative NOMA system by using a dedicated relay and minimized the BS energy consumption. The other is the non-linear model, such as [16]. Specifically, Ref. [16] used the SWIPT technique to ensure the secure transmission for ground users in an unmanned aerial vehicle aided NOMA network. Compared with the linear model, the non-linear model matches the actual circuit scenario better. Due to the complexity of the non-linear models, there exist few related studies.

In this paper, we study a downlink cooperative NOMA system in which a BS serves two paired users. Since there is no direct link between the BS and the far user (due to e.g., physical obstacles or heavy shadowing), the near user acts as a cooperative relay for the far user. However, cooperative relaying may consume extra energy of the near user acting as a relay. Considering the constrained energy, we enable the near user to adopt the SWIPT technique for energy supplement while ensuring relay transmission. Consequently, the energy provided for downlink transmission mainly comes from the BS. By considering the non-linear features of the practical circuits, we adopt a non-linear model for EH. We aim to minimize the BS energy consumption under the required minimum target rates of both users. To achieve this goal, we propose an optimal power-time resource allocation scheme by decoupling the variables properly.

Compared with [15], the innovation of this paper is two-fold. First, we consider a practical non-linear model for EH instead of a simple linear model in [15]. Second, we leverage user relaying to avoid a dedicated relay deployment, and thus decrease system cost.

2 System model

We consider a downlink cooperative NOMA system shown in Figure 1, in which a BS serves two paired users. Due to physical obstacles or heavy shadowing, there is no direct link between the BS and U2. To help information transmission from the BS to U2, the near user U1 acts as a relay for the far user U2. Since the half-duplex relay is easy to implement in practical systems [17,18], U1 works in the half-duplex mode. In particular, U1 has limited battery capacity, and thus first harvests energy from BS signals and then uses all the harvested energy for relaying to prolong its lifetime. As shown in Figure 1, h_1 and h_2 denote respectively the Rayleigh fading channels from BS to U1 and U2, i.e., $h_i \sim \mathcal{CN}\{0, \lambda_i\}, i \in \{1, 2\}$, where λ_i is the variance of h_i.

We adopt a practical non-linear EH model namely constant-linear-constant (CLC) which takes the sensitivity and saturation features of the practical circuits into account [19]. If the BS transmits a special EH signal with power p, the received power at U1 is $p|h_1|^2$. According to the CLC EH model in [20], the harvested energy at U1 can be expressed as

$$E = \begin{cases} 0, & p|h_1|^2 \in [0, P^{\text{sen}}], \\ \eta(p|h_1|^2 - P^{\text{sen}})T_E, & p|h_1|^2 \in [P^{\text{sen}}, P^{\text{sat}}], \\ \eta(P^{\text{sat}} - P^{\text{sen}})T_E, & p|h_1|^2 \in [P^{\text{sat}}, +\infty), \end{cases} \tag{1}$$

where P^{sen} and P^{sat} denote respectively the sensitivity and saturation power threshold of EH, T_E denotes the EH duration, and η $(0 < \eta < 1)$ is the energy conversion efficiency.

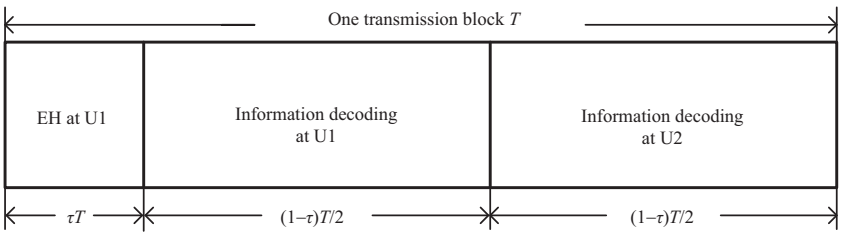

Figure 2 Transmission block structure.

3 Problem description

In this section, we provide the transmission protocol followed by the problem formulation and analysis.

3.1 Transmission protocol

The transmission block structure is shown in Figure 2. In particular, the period of a transmission block is denoted by T, which is divided into three phases, the EH phase with duration τT ($0 \leqslant \tau \leqslant 1$), information decoding phase at U1 with duration $(1-\tau)T/2$, and information decoding phase at U2 with duration $(1-\tau)T/2$.

In the first phase, BS transmits EH signals with power p and the harvested energy E at U1 can be calculated by (1) with $T_E = \tau T$.

In the second phase, the BS transmits a superimposed signal

$$x(t) = \sqrt{\alpha p}x_1(t) + \sqrt{(1-\alpha)p}x_2(t), \tag{2}$$

where p is the BS transmit power, $x_1(t)$ and $x_2(t)$ are respectively the signals with unit power intended to U1 and U2, α ($0 \leqslant \alpha \leqslant 1$) and $(1-\alpha)$ are the power allocation ratios of $x_1(t)$ and $x_2(t)$, respectively. Then, the received signals at U1 can be expressed as

$$y_1(t) = h_1(t)\left[\sqrt{\alpha p}x_1(t) + \sqrt{(1-\alpha)p}x_2(t)\right] + n_1(t), \tag{3}$$

where $n_1 \sim \mathcal{CN}\{0, \sigma^2\}$ denotes additive white Gaussian noise (AWGN) at U1.

Upon receiving the signal from the BS, U1 first decodes x_2 and then decodes x_1 according to the successive interference cancellation (SIC) technique. Consequently, the SINRs that U1 detects x_2 and x_1 can be obtained respectively as

$$\gamma_{12} = \frac{(1-\alpha)p|h_1|^2}{\alpha p|h_1|^2 + \sigma^2}, \tag{4}$$

and

$$\gamma_{11} = \frac{\alpha p|h_1|^2}{\sigma^2}. \tag{5}$$

In the third phase, U1 forwards the decoded x_2 to U2 with all the harvested energy in the first phase. Here, suppose that U1 uses part of the harvested energy for relaying and U2 can successfully decode the required information from U1's relaying, then the harvested energy at U1 from the BS has not been fully utilized in the current time slot. This means, the BS can reduce its transmit power, such that both U1 and U2 can also successfully decode their required information, saving energy at the BS in downlink transmissions. To fully utilize the harvested energy at U1, we enable U1 to use all the harvested energy for relaying.

According to the CLC EH model, the transmit power of U1 can be expressed as

$$p_1 = \frac{2E}{(1-\tau)T} = \begin{cases} 0, & p|h_1|^2 \in [0, P^{\text{sen}}], \\ 2\dfrac{\eta\tau}{(1-\tau)}(p|h_1|^2 - P^{\text{sen}}), & p|h_1|^2 \in [P^{\text{sen}}, P^{\text{sat}}], \\ 2\dfrac{\eta\tau}{(1-\tau)}(P^{\text{sat}} - P^{\text{sen}}), & p|h_1|^2 \in [P^{\text{sat}}, +\infty). \end{cases} \tag{6}$$

Then, the SNR that U2 detects x_2 can be obtained as

$$\gamma_{22} = \frac{p_1|h_2|^2}{\sigma^2}. \tag{7}$$

Consequently, the achievable rates of x_1 and x_2 from the BS to U1 can be obtained as

$$R_{11} = \frac{1}{2}(1-\tau)\log_2(1+\gamma_{11}), \tag{8}$$

and

$$R_{12} = \frac{1}{2}(1-\tau)\log_2(1+\gamma_{12}), \tag{9}$$

respectively. The achievable rate of x_2 from U1 to U2 can be obtained as

$$R_{22} = \frac{1}{2}(1-\tau)\log_2(1+\gamma_{22}). \tag{10}$$

3.2 Problem formulation and analysis

Based on the transmission protocol above, it is straightforward to obtain the BS energy consumption as

$$E_{\rm BS} = p\tau T + p(1-\tau)\frac{T}{2} = p(1+\tau)\frac{T}{2}. \tag{11}$$

We aim to optimize the power-time domain resource (i.e., α, p, and τ) allocation to minimize the BS energy consumption. Meanwhile, we consider minimum rates at both U1 and U2. Without loss of generality, we assume $T = 1$. Thus, we can formulate the power-time resource allocation optimization problem as follows:

$$\min_{\alpha,p,\tau} \quad p\frac{1+\tau}{2} \tag{12a}$$

$$\text{s.t. } R_{12} \geqslant R_2^t,\ R_{11} \geqslant R_1^t, \tag{12b}$$

$$R_{22} \geqslant R_2^t, \tag{12c}$$

$$p \leqslant p^{\max}, \tag{12d}$$

$$0 \leqslant \alpha \leqslant 1,\ 0 \leqslant \tau \leqslant 1, \tag{12e}$$

where R_2^t and R_1^t denote respectively the required minimum rate of x_2 and x_1, $p^{\max}$ is the maximum transmit power of the BS. The constraint (12b) is imposed to ensure that U1 can decode information successfully. The constraint (12c) is built to guarantee that U2 successfully decodes information. The transmit power of the BS, the power allocation factor and the time-switching ratio are restricted by the constraints (12d) and (12e).

4 Resource allocation optimization

We notice that, the variables in (12) are coupled in both the objective function and constraints. It is challenging to solve (12) directly. Then, we solve it by first decoupling these variables and then analytically obtain the optimal solution.

4.1 Optimization of α

Based on the downlink transmission protocol, we first focus on the conditions for success transmission from the BS to U1. Accordingly, the constraint (12b) should be satisfied. By substituting (8) and (9) into (12b), the constraint (12b) becomes

$$[1-\alpha(1+\gamma_{12}^t)]p|h_1|^2 \geqslant \sigma^2\gamma_{12}^t, \tag{13}$$

and

$$\alpha p|h_1|^2 \geqslant \sigma^2\gamma_{11}^t, \tag{14}$$

where $\gamma_{12}^t = 2^{\frac{2R_2^t}{(1-\tau)}} - 1$, and $\gamma_{11}^t = 2^{\frac{2R_1^t}{(1-\tau)}} - 1$. Then, when $0 \leqslant \alpha \leqslant \frac{1}{1+\gamma_{12}^t}$, the constraint (12b) can be transformed as

$$p|h_1|^2 \geqslant \max\{a, b\} \triangleq q(\alpha), \tag{15}$$

where $a = \frac{\sigma^2\gamma_{12}^t}{1-\alpha(1+\gamma_{12}^t)}$, and $b = \frac{\sigma^2\gamma_{11}^t}{\alpha}$. Here, $q(\alpha)$ is the received power threshold of successful decoding at U1. When U1 fails to decode, i.e., $p|h_1|^2 \leqslant q(\alpha)$, U1 keeps silent and the harvested energy at U1 will be locally stored [17, 18]. In this case, the locally stored energy at U1 can be seen as the opportunistic reward for its relaying.

Based on the analysis above, we know that α is only related to the received power threshold of decoding information at U1. Our goal is to minimize the BS energy consumption. Thus, we can obtain the optimal α by minimizing the threshold, i.e.,

$$\min_{\alpha} \quad q(\alpha) = \max\{a, b\} \tag{16a}$$

$$\text{s.t.} \quad 0 \leqslant \alpha \leqslant \frac{1}{1+\gamma_{12}^t}. \tag{16b}$$

Note that, a and b are respectively increasing and decreasing functions of α. In particular, when α approaches to $\frac{1}{1+\gamma_{12}^t}$, a goes to the infinity, and when α approaches to 0, b goes to the infinity. Thus, $q(\alpha)$ reaches its minimum when $a = b$, from which we obtain the optimal power allocation of the BS as [16]

$$\alpha^\star = \frac{\gamma_{11}^t}{\gamma^t}, \tag{17}$$

where $\gamma^t = 2^{\frac{2(R_1^t+R_2^t)}{(1-\tau)}} - 1$. Meanwhile, the minimum value of $q(\alpha)$ is

$$q(\alpha^\star) = \sigma^2\gamma^t. \tag{18}$$

Then, the constraint (15) can be rewritten as

$$p|h_1|^2 \geqslant \sigma^2\gamma^t. \tag{19}$$

4.2 Optimization of p and τ

After ensuring success transfer from the BS to U1, we focus on the conditions required for success transmission from U1 to U2. Therefore, the constraint (12c) should be satisfied. By substituting (10) into (12c), we have

$$p_1 \geqslant \frac{\sigma^2\gamma_{22}^t}{|h_2|^2}, \tag{20}$$

where $\gamma_{22}^t = 2^{\frac{2R_2^t}{(1-\tau)}} - 1$. Note that the constraint (20) contains p_1, which is determined by the received power at U1 as well as the CLC EH model. Since the CLC EH model is a segmented function in terms of the received power, we will discuss the constraint (20) at each segment separately.

4.2.1 $p|h_1|^2 \in [0, P^{\text{sen}}]$

In this case, the U1 transmit power is $p_1 = 0$, which means U1 does not transmit any information.

4.2.2 $p|h_1|^2 \in [P^{\text{sen}}, P^{\text{sat}}]$

In this case, we have $p_1 = 2\frac{\eta\tau}{(1-\tau)}(p|h_1|^2 - P^{\text{sen}})$. Thus, Eq. (20) can be rewritten as

$$p \geqslant \frac{1}{|h_1|^2}\left[P^{\text{sen}} + \frac{\sigma^2}{2\eta|h_2|^2}\frac{(1-\tau)\gamma_{22}^t}{\tau}\right] \triangleq V_1(\tau). \tag{21}$$

Besides, by considering $p|h_1|^2 \geqslant \sigma^2\gamma^t$, the lower bound of p is

$$p \geqslant \max\left\{V_1(\tau), \frac{\sigma^2\gamma^t}{|h_1|^2}\right\} \triangleq V(\tau). \tag{22}$$

Furthermore, the upper bound of p is determined by $p \leqslant p^{\max}$ and $p \leqslant \frac{P^{\text{sat}}}{|h_1|^2}$, i.e.,

$$p \leqslant \min\left\{p^{\max}, \frac{P^{\text{sat}}}{|h_1|^2}\right\} \triangleq c. \tag{23}$$

Consequently, the problem (12) can be transformed as

$$\min_{p,\tau} \quad p\frac{1+\tau}{2} \tag{24a}$$

$$\text{s.t.} \quad V(\tau) \leqslant p \leqslant c, \tag{24b}$$

$$0 \leqslant \tau \leqslant 1. \tag{24c}$$

To guarantee a non-empty feasible set of p, the upper bound should not be smaller than the lower bound, i.e.,

$$V(\tau) = \max\left\{V_1(\tau), \frac{\sigma^2\gamma^t}{|h_1|^2}\right\} \leqslant c, \tag{25}$$

which means $\frac{\sigma^2\gamma^t}{|h_1|^2} \leqslant c$ and $V_1(\tau) \leqslant c$. By substituting $\gamma^t = 2^{\frac{2(R_1^t+R_2^t)}{(1-\tau)}} - 1$ into $\frac{\sigma^2\gamma^t}{|h_1|^2} \leqslant c$, we have

$$\tau \leqslant 1 - \frac{2(R_1^t + R_2^t)}{\log_2(1 + \frac{c|h_1|^2}{\sigma^2})} \triangleq \tau_c, \tag{26}$$

where $\tau_c \geqslant 0$. Meanwhile, $V_1(\tau) \leqslant c$ is equivalent to

$$\phi(\tau) \geqslant 0, \tag{27}$$

where $\phi(\tau) = N\frac{\tau}{1-\tau} - \gamma_{22}^t$ and $N = \frac{2\eta|h_1|^2|h_2|^2}{\sigma^2}(c - \frac{P^{\text{sen}}}{|h_1|^2})$.

Obviously, the objective function in (24) increases monotonically as p increases. Thus, to minimize $p\frac{1+\tau}{2}$, the optimal transmit power is $p = V(\tau)$. Consequently, the problem (24) reduces to a one dimension optimization problem, i.e.,

$$\min_{0\leqslant\tau\leqslant\tau_c} \quad V(\tau)\frac{1+\tau}{2} \tag{28a}$$

$$\text{s.t.} \quad \phi(\tau) \geqslant 0, \tag{28b}$$

which can be solved by the golden ratio search method.

In each search, for a given τ, the solvable probability of the problem (28) can be expressed as

$$\begin{aligned}\Pr\{\phi(\tau) \geqslant 0, 0 \leqslant \tau \leqslant \tau_c\} &= \Pr\left\{V_1(\tau) \leqslant c, \frac{\sigma^2\gamma^t}{|h_1|^2} \leqslant c\right\} = \Pr\left\{|h_1|^2 \geqslant \frac{\sigma^2\gamma^t}{c}, |h_2|^2 \geqslant \frac{\frac{(1-\tau)\sigma^2\gamma_{22}^t}{2\eta\tau}}{c|h_1|^2 - P^{\text{sen}}}\right\}, \\ &= \int_{\frac{\max\{P^{\text{sen}}, \sigma^2\gamma^t\}}{p^{\max}}}^{\frac{P^{\text{sat}}}{p^{\max}}} \frac{1}{\lambda_1} \mathrm{e}^{-\frac{\xi}{\lambda_1} - \frac{\frac{\sigma^2(1-\tau)\gamma_{22}^t}{2\eta\tau\lambda_2}}{(p^{\max}\xi - P^{\text{sen}})}} \mathrm{d}\xi.\end{aligned} \tag{29}$$

4.2.3 $p|h_1|^2 \in [P^{\text{sat}}, +\infty)$

In this case, we have $p_1 = 2\frac{\eta\tau}{(1-\tau)}(P^{\text{sat}} - P^{\text{sen}})$. Consequently, Eq. (20) is equivalent to $\phi(\tau) \geqslant 0$. Considering that $p \geqslant \frac{P^{\text{sat}}}{|h_1|^2}$ and $p \geqslant \frac{\sigma^2\gamma^t}{|h_1|^2}$, the lower bound of p is

$$p \geqslant \max\left\{\frac{P^{\text{sat}}}{|h_1|^2}, \frac{\sigma^2\gamma^t}{|h_1|^2}\right\} \triangleq U(\tau). \tag{30}$$

Then, the problem (12) can be transformed as

$$\min_{p,\tau} \quad p\frac{1+\tau}{2} \tag{31a}$$

$$\text{s.t.} \quad U(\tau) \leqslant p \leqslant p^{\max}, \tag{31b}$$

$$\phi(\tau) \geqslant 0, \tag{31c}$$

$$0 \leqslant \tau \leqslant 1. \tag{31d}$$

To guarantee a non-empty feasible set of p, the lower bound $U(\tau)$ of p should be smaller than the upper bound $p^{\max}$, i.e., $U(\tau) \leqslant p^{\max}$, which yields $\tau \leqslant \tau_c$. Similarly, to minimize $p\frac{1+\tau}{2}$, the optimal transmit power is $p = U(\tau)$.

Consequently, Eq. (31) reduces to a one-dimension optimization problem, i.e.,

$$\min_{0\leqslant\tau\leqslant\tau_c} U(\tau)\frac{1+\tau}{2} \tag{32a}$$

$$\text{s.t.} \quad \phi(\tau) \geqslant 0, \tag{32b}$$

which can be also solved by the golden ratio search method.

In each search, for a given τ, the solvable probability of the problem (32) can be expressed as

$$\begin{aligned}\Pr\{0 \leqslant \tau \leqslant \tau_c, \phi(\tau) \geqslant 0\} &= \Pr\left\{|h_1|^2 \leqslant \frac{\max\{P^{\text{sat}}, \sigma^2\gamma^t\}}{p^{\max}}, |h_2|^2 \geqslant \frac{(1-\tau)\sigma^2\gamma_{22}^t}{2\eta\tau(P^{\text{sat}} - P^{\text{sen}})}\right\}, \\ &= \mathrm{e}^{-\frac{\max\{P^{\text{sat}}, \sigma^2\gamma^t\}}{\lambda_1 p} - \frac{\frac{\sigma^2(1-\tau)\gamma_{22}^t}{2\eta\tau\lambda_2}}{(P^{\text{sat}} - P^{\text{sen}})}}.\end{aligned} \tag{33}$$

4.2.4 *Solvable probability of the problem (12)*

According to the analysis above, as long as one of the problems (24) and (31) is solvable, the problem (12) is solvable. Thus, for a given τ in each search, the solvable probability of the problem (12) can be expressed as

$$\begin{aligned}\mathcal{P}_{\text{solvable}} &= \Pr\{0 \leqslant \tau \leqslant \tau_c, \phi(\tau) \geqslant 0\} \\ &= \int_{\frac{\max\{P^{\text{sen}}, \sigma^2\gamma^t\}}{p^{\max}}}^{\frac{P^{\text{sat}}}{p^{\max}}} \frac{1}{\lambda_1}\mathrm{e}^{-\frac{\xi}{\lambda_1} - \frac{\frac{\sigma^2(1-\tau)\gamma_{22}^t}{2\eta\tau\lambda_2}}{(p^{\max}\xi - P^{\text{sen}})}}\mathrm{d}\xi + \mathrm{e}^{-\frac{\max\{P^{\text{sat}}, \sigma^2\gamma^t\}}{\lambda_1 p} - \frac{\frac{\sigma^2(1-\tau)\gamma_{22}^t}{2\eta\tau\lambda_2}}{(P^{\text{sat}} - P^{\text{sen}})}} \\ &= \begin{cases} \int_{\frac{P^{\text{sen}}}{p^{\max}}}^{\frac{P^{\text{sat}}}{p^{\max}}} \frac{\mathrm{e}^{-\frac{\xi}{\lambda_1} - \frac{\frac{\sigma^2(1-\tau)\gamma_{22}^t}{2\eta\tau}}{(p^{\max}\xi - P^{\text{sen}})}}}{\lambda_1}\mathrm{d}\xi + \mathrm{e}^{-\frac{P^{\text{sat}}}{\lambda_1 p^{\max}} - \frac{\frac{\sigma^2(1-\tau)\gamma_{22}^t}{2\eta\tau\lambda_2}}{(P^{\text{sat}} - P^{\text{sen}})}}, & \sigma^2\gamma^t \in [0, P^{\text{sen}}], \\ \int_{\frac{\sigma^2\gamma^t}{p^{\max}}}^{\frac{P^{\text{sat}}}{p^{\max}}} \frac{\mathrm{e}^{-\frac{\xi}{\lambda_1} - \frac{\frac{\sigma^2(1-\tau)\gamma_{22}^t}{2\eta\tau}}{(p^{\max}\xi - P^{\text{sen}})}}}{\lambda_1}\mathrm{d}\xi + \mathrm{e}^{-\frac{P^{\text{sat}}}{\lambda_1 p^{\max}} - \frac{\frac{\sigma^2(1-\tau)\gamma_{22}^t}{2\eta\tau\lambda_2}}{(P^{\text{sat}} - P^{\text{sen}})}}, & \sigma^2\gamma^t \in [P^{\text{sen}}, P^{\text{sat}}], \\ \mathrm{e}^{-\frac{\sigma^2\gamma^t}{\lambda_1 p^{\max}} - \frac{\frac{\sigma^2(1-\tau)\gamma_{22}^t}{2\eta\tau\lambda_2}}{(P^{\text{sat}} - P^{\text{sen}})}}, & \sigma^2\gamma^t \in [P^{\text{sat}}, +\infty), \\ 0, & \text{otherwise.} \end{cases}\end{aligned} \tag{34}$$

4.3 Algorithm summary and complexity analysis

Based on the analysis above, the algorithm for solving the optimal value of (12) follows three steps. First, construct the optimization problem (28) and (32). Second, if (28) and/or (32) are solvable, obtain the corresponding optimal τ^* with the one-dimension golden ratio search method. Third, calculate the corresponding optimal p^* with $V(\tau^*)$ or $U(\tau^*)$, and calculate the optimal α^* with (17). Specially, if both (28) and (32) are solvable, select the optimal solution subject to the lower BS energy consumption.

The complexity of the algorithm is dominated by the one-dimension search process. If the search accuracy is ϵ, the number of iterations required for convergence is at least $\log_2(\frac{1+\tau_c}{\epsilon})$. Accordingly, the computational complexity of the proposed algorithm is $O(\log_2 \frac{1+\tau_c}{\epsilon})$.

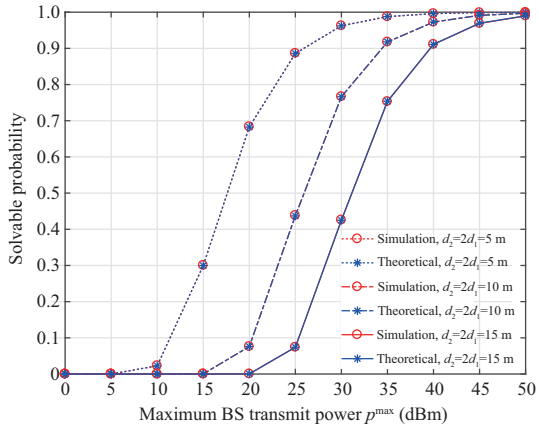

Figure 3 (Color online) Solvable probability versus $p^{\max}$ (dBm) for different distances, where $\tau = 0.1$ and $R_1^t = 2R_2^t = 0.2$ (bps/Hz).

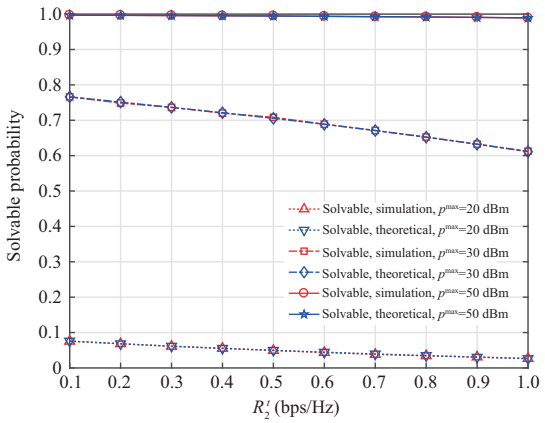

Figure 4 (Color online) Solvable probability versus R_2^t (bps/Hz), where $R_1^t = 2R_2^t$, $\tau = 0.1$, and $d_2 = 2d_1 = 10$ (m).

5 Numerical results

In this section, we provide simulation results to show the system performance for the downlink SWIPT-assisted cooperative NOMA system. We assume the path loss model of the channel as $\lambda_i = \rho d_i^{-\omega}$, where $\rho = 10^{-3}$, the path loss exponent $\omega = 2.7$ [16], d_1 and d_2 denote the distances from the BS to U1 and from U1 to U2. Similar to [20], we set the energy conversion efficiency $\eta = 0.7$, the noise power as $\sigma^2 = -100$ (dBm), the sensitivity threshold $P^{\text{sen}} = -25$ (dBm), the saturation threshold $P^{\text{sat}} = -5$ (dBm). We obtain each simulation result by averaging 100k independent trials.

Figure 3 shows the solvable probability versus $p^{\max}$ for different distances. From the figure, we observe that the theoretical curve of solvable probability matches well with the simulation curve of solvable probability. This verifies the correctness of the theoretical analysis in (34). Besides, we observe that the solvable probability increases as the distance grows. This is because a longer distance requires a higher BS transmit power to ensure success transmission.

Figure 4 illustrates the solvable probability versus R_2^t. From the figure, we observe that the theoretical curve of solvable probability matches well with the simulation curve of solvable probability, which also verifies the correctness of the theoretical analysis in (34). Besides, we observe that the solvable probability decreases as the required minimum rate grows. This is because the higher the required minimum rate is, the harder it is to transfer information successfully, reducing the solvable probability. Furthermore, we observe that the solvable probability increases as the maximum BS transmit power grows. This is reasonable since a larger transmit power promotes successful transmission, which increases the solvable probability.

Figure 5 illustrates the minimum BS energy consumption versus $p^{\max}$ for different distances. From the figure, we observe that the curve of the proposed scheme matches well with the optimal scheme which obtained by the enumeration search. This verifies that the proposed scheme is the optimal scheme for minimizing BS energy consumption and has a low complexity. Besides, we observe that the curve of the minimum BS energy consumption increases as $p^{\max}$. This can be explained as follows. When $p^{\max}$ is small, the transmit power of U1 for successful transmission increases as $p^{\max}$ grows, which consumes more energy of the BS. When $p^{\max}$ is large, the transmit power of U1 remains constant as $p^{\max}$ grows. This is because the harvested energy at U1 will gradually flatten due to the saturation effect of practical circuits. Besides, we observe that the minimum BS energy consumption increases as the distance grows. This is straightforward that a longer distance may need a larger transmit power to compensate the path loss and thus leads to a higher BS energy consumption.

Figure 6 illustrates the minimum BS energy consumption versus $p^{\max}$ with distinct minimum required rates. From the figure, we observe that the curve of the minimum BS energy consumption increases as $p^{\max}$. The reason can be explained as follows. If $p^{\max}$ is small, the transmit power of U1 for success transmission increases as $p^{\max}$ grows, which consumes more BS energy. If $p^{\max}$ is large, the transmit power of U1 remains constant as $p^{\max}$ grows. This is because the harvested energy at U1 will no longer continue to increase due to the saturation effect of practical circuits. Besides, we observe that the minimum BS

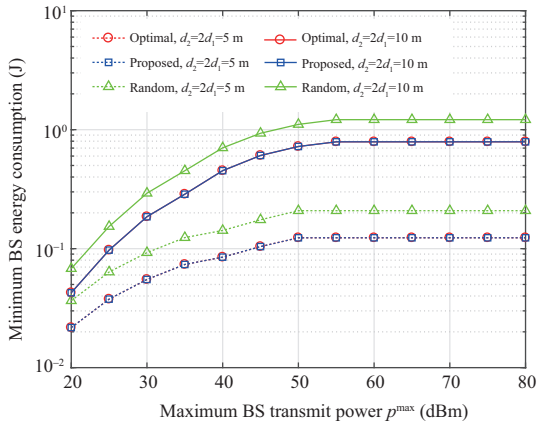

Figure 5 (Color online) Minimum BS energy consumption versus $p^{\max}$ (dBm) for different distances, where $R_1^t = 2R_2^t = 0.2$ (bps/Hz).

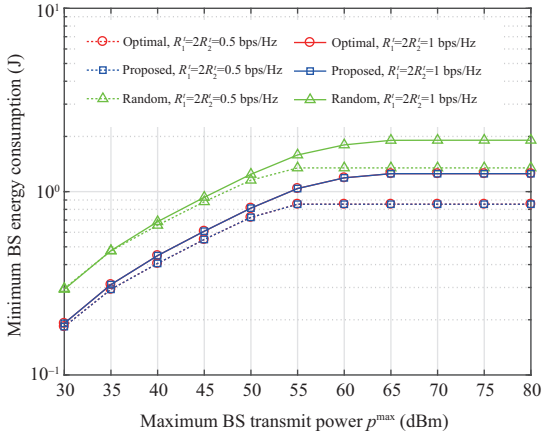

Figure 6 (Color online) Minimum BS energy consumption versus $p^{\max}$ (dBm) with distinct minimum required rates, where $d_1 = d_2 = 5$ (m).

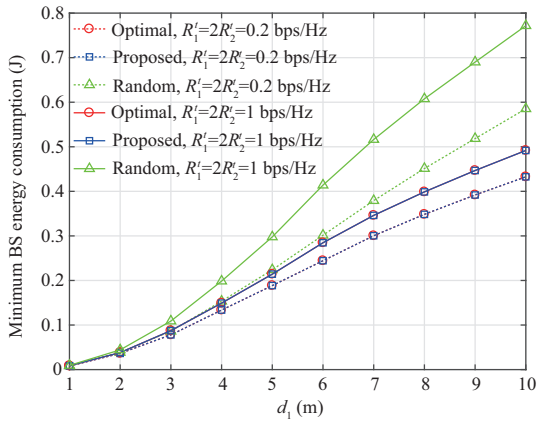

Figure 7 (Color online) Minimum BS energy consumption versus d_1 (m), where $d_2 = 2d_1$ and $p^{\max} = 30$ (dBm).

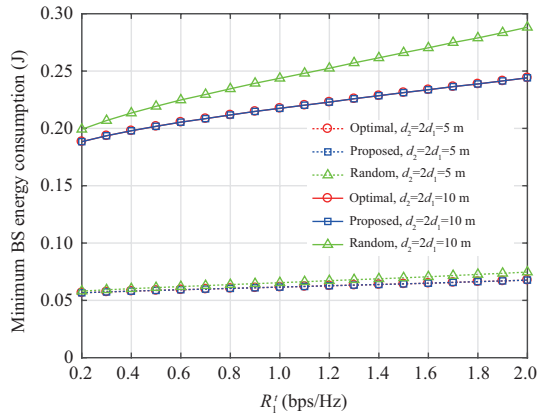

Figure 8 (Color online) Minimum BS energy consumption versus R_1^t (bps/Hz), where $R_2^t = R_1^t/2$ and $p^{\max} = 30$ (dBm).

energy consumption increases as the required minimum rate grows. This is reasonable because a higher required minimum rate needs a larger transmit power to satisfy success transmission conditions and thus results in a higher BS energy consumption.

Figure 7 reveals the relationship between the minimum BS energy consumption and d_1. From the figure, we observe that the curve of the minimum BS energy consumption increases as d_1 grows. This is straightforward that a longer distance may need a larger transmit power to compensate the path loss and thus leads to a higher BS energy consumption. Besides, we observe that the minimum BS energy consumption increases as the required minimum rate grows. This is because a higher required minimum rate for success transmission needs more BS energy.

Figure 8 provides the minimum BS energy consumption versus R_1^t. From the figure, we observe that the curve of the minimum BS energy consumption increases as the required minimum rate R_1^t. This is reasonable since a higher minimum required rate is more difficult to meet the success transmission condition, increasing the BS energy consumption. Furthermore, we observe that the minimum BS energy consumption increases as the distance grows. This makes sense because a higher maximum BS transmit power can satisfy the required minimum rate constraints of users in worse channel conditions, and consumes more BS energy.

6 Conclusion

In this paper, we studied a downlink cooperative NOMA system in which a BS serves two paired users on the same frequency band simultaneously. In particular, the near user acts as an energy-constrained relay for the far user with the SWIPT technique. By adopting a practical non-linear EH model, we proposed an optimal power-time resource allocation algorithm and minimized the BS energy consumption. Simulation results verified the theoretical analysis and showed the system performance.

Acknowledgements This work was supported by the Young Talent Support Project of China Association for Science and Technology (CAST).

References

1 Zhang L, Liang Y C, Niyato D. 6G visions: mobile ultra-broadband, super Internet-of-Things, and artificial intelligence. China Commun, 2019, 16: 1–14
2 Guo F, Yu F R, Zhang H, et al. Enabling massive IoT toward 6G: a comprehensive survey. IEEE Int Things J, 2021, 8: 11891–11915
3 Lin J, Yu W, Zhang N, et al. A survey on Internet of Things: architecture, enabling technologies, security and privacy, and applications. IEEE Int Things J, 2017, 4: 1125–1142
4 Dawy Z, Saad W, Ghosh A, et al. Toward massive machine type cellular communications. IEEE Wirel Commun, 2017, 24: 120–128
5 Zhai D, Zhang R, Cai L, et al. Energy-efficient user scheduling and power allocation for NOMA-based wireless networks with massive IoT devices. IEEE Int Things J, 2018, 5: 1857–1868
6 Jiao J, Liao S Y, Sun Y Y, et al. Fairness-improved and QoS-guaranteed resource allocation for NOMA-based S-IoT network. Sci China Inf Sci, 2021, 64: 169306
7 Kim J B, Lee I H. Non-orthogonal multiple access in coordinated direct and relay transmission. IEEE Commun Lett, 2015, 19: 2037–2040
8 Pang X W, Tang J, Zhao N, et al. Energy-efficient design for mmWave-enabled NOMA-UAV networks. Sci China Inf Sci, 2021, 64: 140303
9 Li Y, Li Y, Chu X, et al. Performance analysis of relay selection in cooperative NOMA networks. IEEE Commun Lett, 2019, 23: 760–763
10 Zhang Z Q, Ma Z, Xiao M, et al. Full-duplex device-to-device aided cooperative non-orthogonal multiple access. IEEE Trans Veh Technol, 2017, 66: 4467–4471
11 Zhang L, Liu J, Xiao M, et al. Performance analysis and optimization in downlink NOMA systems with cooperative full-duplex relaying. IEEE J Sel Areas Commun, 2017, 35: 2398–2412
12 Liu Y, Ding Z, Elkashlan M, et al. Cooperative non-orthogonal multiple access with simultaneous wireless information and power transfer. IEEE J Sel Areas Commun, 2016, 34: 938–953
13 Liu M J, Feng G, Zhuang W H. Energy-efficient URLLC service provisioning in softwarization-based networks. Sci China Inf Sci, 2021, 64: 182302
14 Yuan Y, Xu Y, Yang Z, et al. Energy efficiency optimization in full-duplex user-aided cooperative SWIPT NOMA systems. IEEE Trans Commun, 2019, 67: 5753–5767
15 Li G, Mishra D, Hu Y, et al. Optimal designs for relay-assisted NOMA networks with hybrid SWIPT scheme. IEEE Trans Commun, 2020, 68: 3588–3601
16 Wang W, Tang J, Zhao N, et al. Joint precoding optimization for secure SWIPT in UAV-aided NOMA networks. IEEE Trans Commun, 2020, 68: 5028–5040
17 Nasir A A, Zhou X, Durrani S, et al. Relaying protocols for wireless energy harvesting and information processing. IEEE Trans Wirel Commun, 2013, 12: 3622–3636
18 Atapattu S, Evans J. Optimal energy harvesting protocols for wireless relay networks. IEEE Trans Wirel Commun, 2016, 15: 5789–5803
19 Alevizos P N, Bletsas A. Sensitive and nonlinear far-field RF energy harvesting in wireless communications. IEEE Trans Wirel Commun, 2018, 17: 3670–3685
20 Hakimi A, Mohammadi M, Mobini Z, et al. Full-duplex non-orthogonal multiple access cooperative spectrum-sharing networks with non-linear energy harvesting. IEEE Trans Veh Technol, 2020, 69: 10925–10936